

## APPLIED PHYSICS

# A polarization-induced 2D hole gas in undoped gallium nitride quantum wells

Reet Chaudhuri<sup>1\*</sup>, Samuel James Bader<sup>2</sup>, Zhen Chen<sup>2</sup>, David A. Muller<sup>2,4</sup>,  
Huili Grace Xing<sup>1,3,4</sup>, Debdeep Jena<sup>1,3,4</sup>

A high-conductivity two-dimensional (2D) hole gas, analogous to the ubiquitous 2D electron gas, is desirable in nitride semiconductors for wide-bandgap p-channel transistors. We report the observation of a polarization-induced high-density 2D hole gas in epitaxially grown gallium nitride on aluminium nitride and show that such hole gases can form without acceptor dopants. The measured high 2D hole gas densities of about  $5 \times 10^{13}$  per square centimeters remain unchanged down to cryogenic temperatures and allow some of the lowest p-type sheet resistances among all wide-bandgap semiconductors. The observed results provide a probe for studying the valence band structure and transport properties of wide-bandgap nitride interfaces.

The high-conductivity quantum-confined two-dimensional (2D) electron gases (2DEGs) at the interface of AlGaIn/GaN semiconductor heterostructures, discovered in the mid-1990s (1), did not require the presence of chemical dopants. The origin of the 2DEG was tracked down to the existence of broken inversion symmetry along the [0001] axis of gallium nitride (GaN), combined with the high polarity of the metal-nitrogen bond in GaN and aluminium nitride (AlN) (2, 3). These properties, as well as the tensile epitaxial strain of AlN on GaN, lead to the presence of spontaneous  $P_{sp}$  and piezoelectric  $P_{pz}$  polarization in AlN/GaN heterostructures (4). The polarization difference  $[(P_{sp}^{AlN} + P_{pz}^{AlN}) - P_{sp}^{GaN}] \cdot \hat{n} = \sigma_{\pi}$  constitutes a net-positive fixed-polarization sheet charge. This charge, with the potential barrier of a large conduction band offset, induces a 2DEG at such a heterojunction, without any chemical doping. The carrier concentration that can be induced by the polar discontinuity far exceeds what is achievable in the bulk with chemical doping or at junctions with modulation doping. Such robust polarization-induced 2DEGs in Al(Ga)N/GaN heterojunctions have been investigated for the past two decades and contributed to several applications, such as ultrafast unipolar transistors and sensors (5, 6).

However, the p-type analog of the undoped polarization-induced 2DEG—the undoped 2D hole gas (2DHG)—has remained elusive. Although low-density 2D and 3D hole gases have been previously inferred in nitride heterojunctions in several reports (7–16), they have been either modulation Mg-doped heterostructures or structures

in which both mobile electrons and holes are present. Substantial advances in energy-efficient wide-bandgap electronics are expected for GaN/AlN-based high-voltage complementary switches (17), if a high-conductivity undoped 2DHG can be generated.

In contrast to the 2DEG structure, if a thin layer of metal-polar GaN is grown on a relaxed AlN substrate, the net interface polarization difference,  $[(P_{sp}^{GaN} + P_{pz}^{GaN}) - P_{sp}^{AlN}] \cdot \hat{n} = \sigma_{\pi}$ , is negative in sign and should induce holes. The valence band offset of AlN and GaN confines the 2DHG, as schematically shown in the energy band diagram of Fig. 1A, a self-consistent solution of a multiband  $k \cdot p$  and Poisson equations (18). A mobile 2D hole gas of sheet density roughly equal to the fixed interface polarization charge  $\sigma_{\pi} \sim 5 \times 10^{13} \text{ cm}^{-2}$  is expected to form at the heterojunction, depending on the thickness of the GaN layer.

The schematic of GaN/AlN layer structures, which we grew using molecular beam epitaxy (MBE), is shown in Fig. 1B (19). We observed a sharp heterojunction between wurtzite GaN and AlN, with the GaN layer pseudomorphically strained (Fig. 1, C and D) (20). Further structural and chemical details are shown in Fig. 2. The as-grown surface has a smooth morphology, with clearly resolved atomic steps (Fig. 2A). The fringes and multiple peaks of the x-ray diffraction spectrum (Fig. 2B) indicate a smooth, uniform heterostructure over the entire millimeter-scale beam size. This was further corroborated by the large-area scanning transmission electron microscopy (STEM) images in fig. S1. A reciprocal-space x-ray map indicates that the GaN epitaxial layer is fully, biaxially, compressively strained (by 2.4%) to the underlying AlN layer (Fig. 2C). Thus, the heterostructure is structurally and chemically in a form that should exhibit the undoped polarization-induced 2DHG (Figs. 1 and 2), and the transport studies discussed next indicate that this is the case.

The layer structure of three samples is shown in Fig. 3A: Sample A is an undoped ~13-nm GaN

layer on AlN. Sample B is identical to A, except that the top 10 nm of GaN are doped with Mg to lock the Fermi level to valence band edge separation, screening the 2DHG from variations of the surface potential. For comparison with conventional acceptor doping, a thick Mg-doped GaN (sample C) was also measured. The temperature-dependent Hall-effect transport properties of the three samples are shown in Fig. 3, A to C, measured from 300 to 10 K. The mobile charge density  $n_s = IB/qV_H$  is obtained from the Hall voltage  $V_H$  that develops upon driving a current  $I$  through the 2D hole gas in a magnetic field  $B$  perpendicular to its plane. The Hall voltage results from the Lorentz force  $F = q(v \times B)$ , which drives holes in a direction opposite to electrons, leading to a positive sign. The carrier mobility  $\mu_p = 1/qn_s R_s$  is obtained from the measured sheet resistance  $R_s$ . The positive slope of the Hall resistance ( $V_H/I$ ) versus magnetic field and positive Hall-coefficient sign for all samples in this study ensured that we were studying and comparing only holes.

The resistivity of the Mg-doped bulk GaN control sample C increases sharply with the lowering of temperature from ~40 kilohms/square at 300 K to 2 megohms/square at ~180 K (Fig. 3A). This increase in resistivity is almost entirely caused by the ~100× decrease of the thermally generated mobile hole density, which freezes out with an activation energy  $E_A \sim 170$  meV (Fig. 3B). We observed a dramatically different behavior for the undoped heterostructure sample A and the Mg-doped heterostructure B. They showed metallic behavior, with the resistivity decreasing with decreasing temperature, which is a signature of a degenerate 2D hole gas.

The resistivity of heterostructure A decreased from ~6.0 kilohm/square at 300 K to ~1 kilohm/square at 10 K, and the resistivity of heterostructure B decreased from ~8.0 kilohm/square at 300 K to ~2 kilohm/square at 20 K (Fig. 3A). Because the hole densities measured in samples A and B are nearly independent of temperature (Fig. 3B), all the change in the resistivity was caused by an increase in the hole mobility as the temperature was lowered. The high hole sheet densities measured are similar for the doped and undoped heterostructures in samples A and B because the integrated acceptor sheet density in sample B is only  $\sim 5 \times 10^{12} \text{ cm}^{-2}$ , which is about an order of magnitude lower than the measured mobile hole gas density. This direct measurement, without any other parallel 2DEG or 3D hole channels, thus points to the presence of a high-density polarization-induced 2D hole gas in the undoped heterojunction. Contactless wafer-scale sheet resistivity measurements shown in fig. S3 confirm the presence of the hole gas in the undoped structures, corroborating that holes are polarization-induced and exist at the heterojunction independent of whether metal layers are deposited on the surface.

The mobility of the 2D hole gas in the undoped heterostructure increases from ~25  $\text{cm}^2/\text{V}\cdot\text{s}$  at 300 K to ~190  $\text{cm}^2/\text{V}\cdot\text{s}$  at 10 K and in the doped heterostructure increases from ~20  $\text{cm}^2/\text{V}\cdot\text{s}$  at

<sup>1</sup>School of Electrical and Computer Engineering, Cornell University, Ithaca, NY 14853, USA. <sup>2</sup>School of Applied and Engineering Physics, Cornell University, Ithaca, NY 14853, USA. <sup>3</sup>Department of Materials Science and Engineering, Cornell University, Ithaca, NY 14853, USA. <sup>4</sup>Kavli Institute at Cornell for Nanoscale Science, Cornell University, Ithaca, NY 14853, USA.

\*Corresponding author. Email: rtc77@cornell.edu

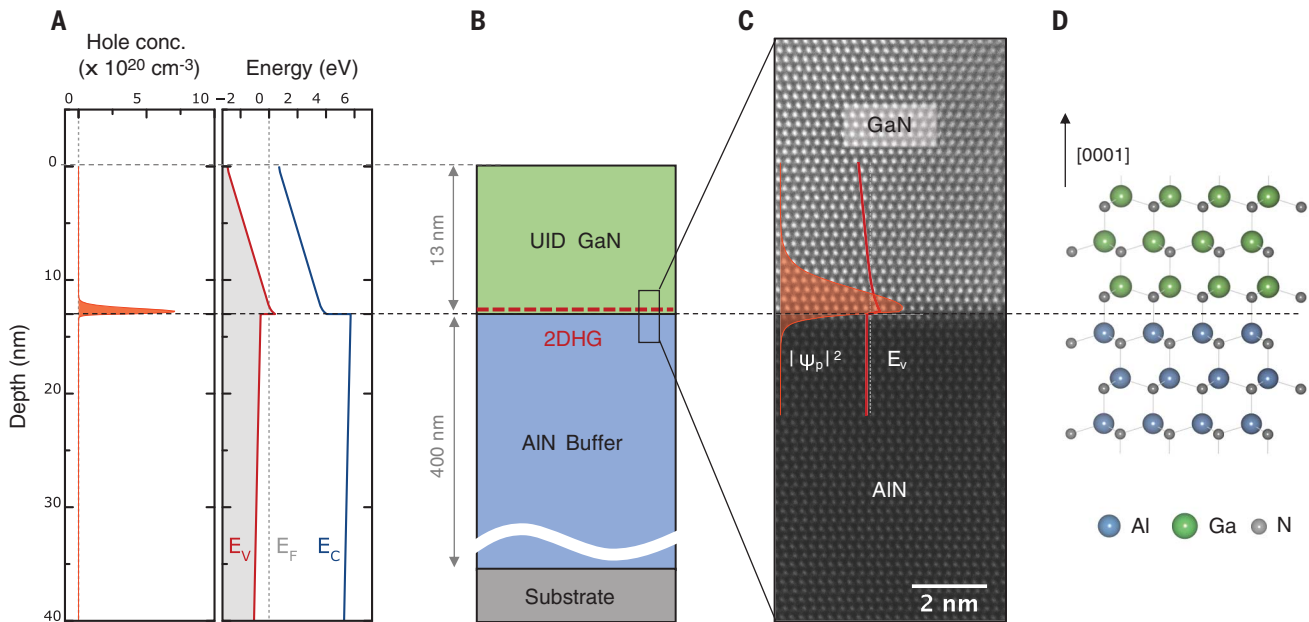


**Fig. 1. Epitaxially grown GaN/AlN heterostructures.** (A) Energy-band diagram of a 13-nm undoped GaN on AlN heterostructure, showing the formation of a quantum well in the valence band and the high-density of confined holes accumulated at the GaN/AlN interface. (B) Schematic of the epitaxially grown layer structure. (C) High-

resolution STEM image showing the metal-polar wurtzite crystalline lattice of the heterointerface. The valence band edge, and probability density of the holes from (A) are overlaid on the interface. (D) Schematic of the metal-polar GaN/AlN heterointerface (20), corresponding to the STEM image in (C).

300 K to  $\sim 120 \text{ cm}^2/\text{V}\cdot\text{s}$  at 20 K, an increase of  $\sim 6\times$  to  $7\times$  (Fig. 3C). The variation of the measured 2D hole gas mobility with temperature is expected to be strongly influenced by acoustic phonon scattering (21), in addition to the polar optical phonon scattering that dominates in most polar compound semiconductors. Although the hole mobilities do not saturate at  $\sim 10$  K, an extrapolation points to values in the range of  $\sim 200 \text{ cm}^2/\text{V}\cdot\text{s}$ . Because the 2D hole gas density survives to cryogenic temperatures, magneto-transport studies can be used to directly access and probe the nature of the valence band of GaN.

We observed the 2DHGs in multiple samples similar to samples A and B with reproducible properties (table S1). As further evidence for the polarization-induced origin of the 2D hole gas, the variation of the density of the 2D hole gas with the thickness of the GaN layer is shown in fig. S2, marking a well-defined critical thickness. This is the exact dual of what is observed in the undoped polarization-induced Al(Ga)N/GaN 2DEG (22) and provides a valuable degree of freedom for p-channel transistor design.

How do the observed polarization-induced 2D hole gases in the undoped and doped GaN/AlN heterostructures compare with those reported in nitride semiconductors and in general with hole gases across various semiconductor material systems? The 2DHG densities of  $\sim 5 \times 10^{13} \text{ cm}^{-2}$  measured in this work (listed in table S1) are near the expected polarization difference and much higher than previously reported 2DHG densities in nitride semiconductors (Fig. 4A) (8–15). The hole densities are among the highest among all

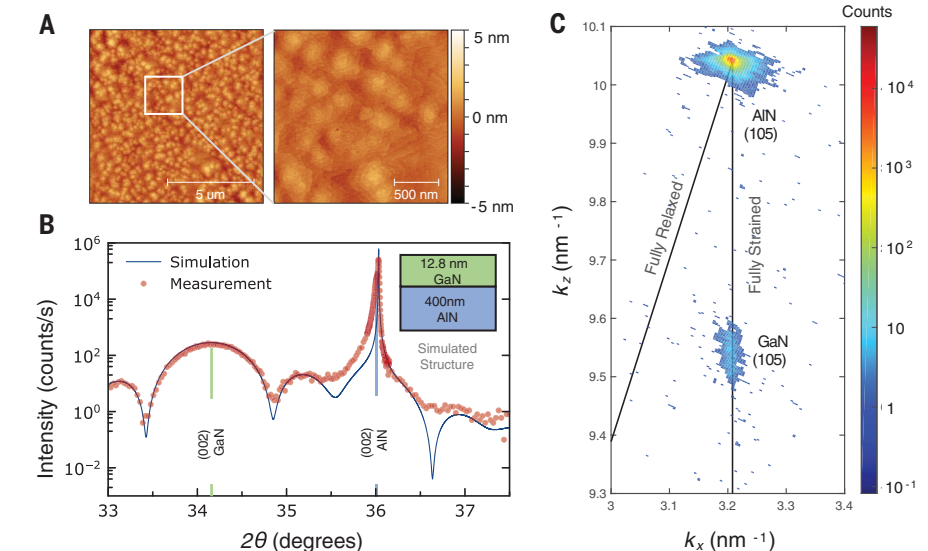


**Fig. 2. Structural properties of the MBE-grown GaN/AlN heterostructures.** (A) Atomic force microscopy (AFM) scans of the as-grown surface. The root mean square roughnesses are  $\sim 0.69$  and  $\sim 0.46$  nm for the 10 and 2  $\mu\text{m}$  scans, respectively. (B) X-ray diffraction (XRD)  $2\theta$  scan across the symmetric (002) reflection and the simulated data (19), confirming the targeted thicknesses and sharp interfaces. (C) Reciprocal space map scan of the asymmetric (105) reflections of GaN and AlN shows that the 13-nm GaN layer is fully strained to the AlN layer.

semiconductor systems, including GaAs/AlGaAs (23, 24), SrTiO<sub>3</sub>/LaAlO<sub>3</sub> (25), surface-conducting diamond (26–30), heterostructures with Ge channels (31–35), Si inversion channels (36), and heterostructures with GaSb channels (37–39), as

shown in Fig. 4B. The high 2D hole density in the nitride leads to some of the lowest sheet resistances, despite lower hole mobilities.

The 2DHG mobilities in the wide-bandgap nitrides are not comparatively high because of

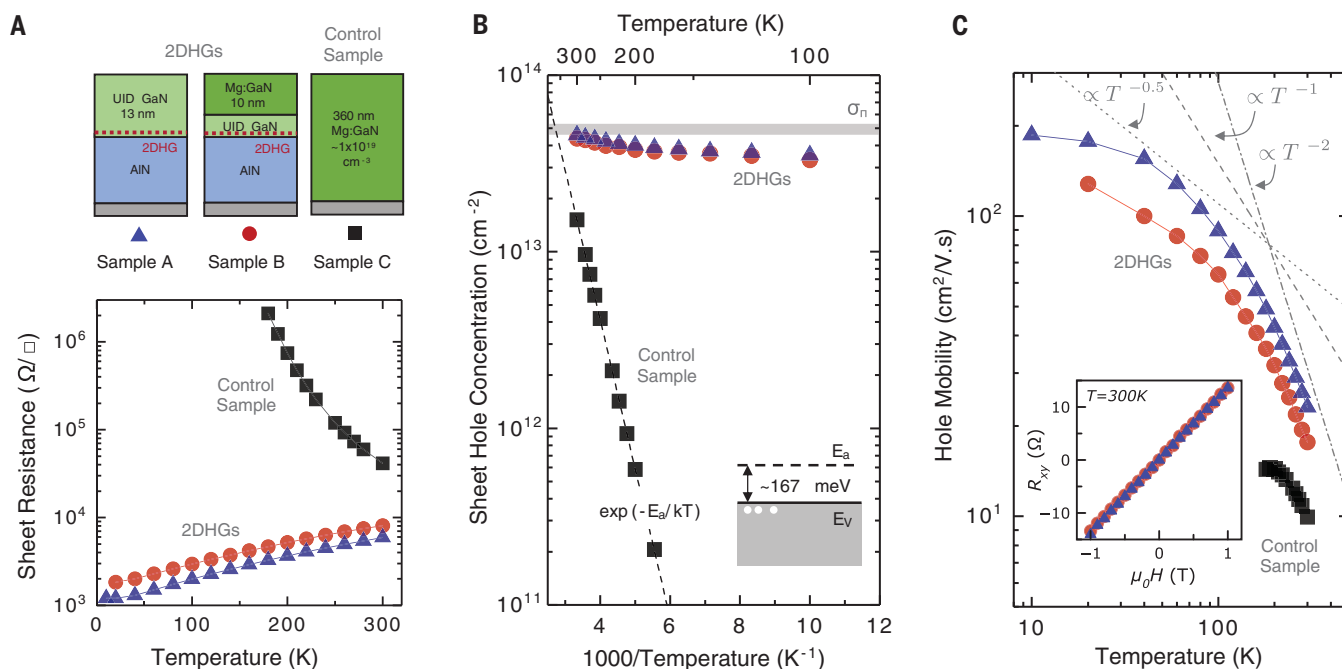
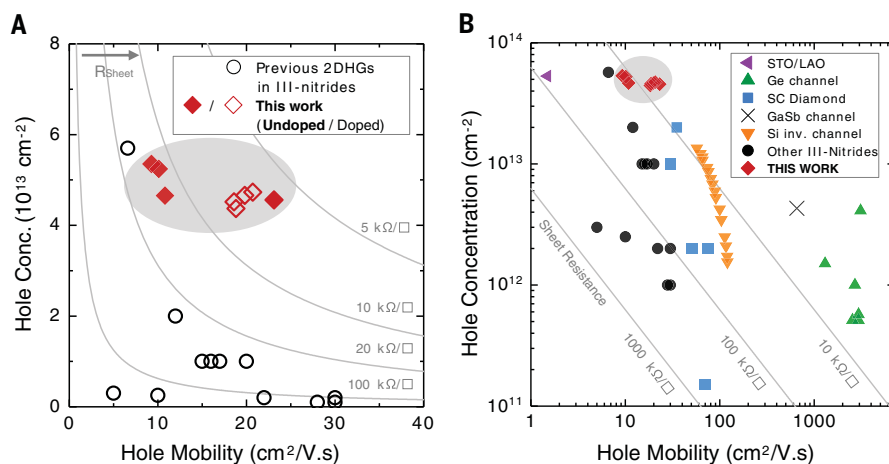


**Fig. 3. Temperature-dependent magnetotransport measurements.** Shown are the data from 300 to 10 K at 1 T magnetic field of 2DHG samples A and B, along with a Mg-doped GaN control sample C. **(A)** The 2DHG samples A and B exhibit a metallic behavior of decreasing sheet resistance with decreasing temperature, whereas the control sample C is insulating in behavior, becoming too resistive below  $\sim 180$  K for measurement. **(B)** The measured mobile hole concentrations over a range of temperatures in samples A, B, and C. In the Mg-doped

GaN (sample C), holes freeze out below 180 K. The density in the 2DHG of samples A and B show almost no change in the hole concentration down to cryogenic temperatures. **(C)** The measured hole mobilities in samples A, B, and C for a range of temperatures. The 2DHG in samples A and B show higher mobilities than that of C. (Inset) Hall resistance versus magnetic field measured at room temperature indicates a positive Hall coefficient (holes) in both samples A and B.

**Fig. 4. Comparison of room-temperature transport properties of 2D hole gases with prior work.** **(A)** Comparison with previously reported 2DHGs in nitride heterostructures (8–14) (open symbols indicate Mg-typed doping). The doped as well as undoped structures reported in this work have much higher hole densities and decent mobilities, enabling record high p-type conductivity of  $\sim 6$  kilohms/square. **(B)** Comparing across other semiconductor material systems such as oxides  $\text{SrTiO}_3/\text{LaAlO}_3$  (25), surface conducting diamond (26–29), Ge channels (31–35), Si inversion channels (36), and GaSb channels (37), this work has the highest room-temperature hole density and the highest conductivities among wide-bandgap semiconductors (III-nitrides, oxides, and diamond), the latter of which is critical for high-performing lateral power devices.



the high effective mass of both heavy and light holes in GaN (40). However, a large bandgap means that the high 2D hole gas densities can be modulated effectively with a gate through field effect because the semiconductor intrinsically is capable of sustaining much larger electric fields. Because of the fundamentally different origin of the 2DHG in the nitrides, this form of doping is expected to scale down to the individual unit cells of the semiconductor crystal and not be

affected by random dopant fluctuations in case of Mg-doping in GaN.

Mg acceptor doping was a key breakthrough in making GaN photonics feasible (41); however, the experimental observation of the polarization-induced undoped 2D hole gas in this work shows that Mg acceptor doping is not compulsory for the generation of holes in nitride semiconductors. The internal broken-symmetry-induced polarization fields have enough strength to provide holes

of very high densities, with several potential scientific and technological applications.

#### REFERENCES AND NOTES

- M. A. Khan, J. N. Kuznia, J. M. Van Hove, N. Pan, J. Carter, *Appl. Phys. Lett.* **60**, 3027–3029 (1992).
- O. Ambacher et al., *J. Appl. Phys.* **85**, 3222–3233 (1999).
- F. Bernardini, V. Fiorentini, D. Vanderbilt, *Phys. Rev. B Condens. Matter* **56**, R10024–R10027 (1997).
- C. Wood, D. Jena, Eds., *Polarization Effects in Semiconductors: From Ab Initio Theory to Device Applications* (Springer, 2007).

5. S. J. Pearton *et al.*, *J. Phys. Condens. Matter* **16**, R961–R994 (2004).
6. U. K. Mishra, L. Shen, T. E. Kazior, Y.-F. Wu, *Proc. IEEE* **96**, 287–305 (2008).
7. T. Zimmermann *et al.*, *IEEE Electron Device Lett.* **25**, 450–452 (2004).
8. R. Chu, Y. Cao, M. Chen, R. Li, D. Zehnder, *IEEE Electron Device Lett.* **37**, 269–271 (2016).
9. K. Zhang, M. Sumiya, M. Liao, Y. Koide, L. Sang, *Sci. Rep.* **6**, 23683 (2016).
10. H. Hahn *et al.*, *IEEE Trans. Electron Dev.* **60**, 3005–3011 (2013).
11. B. Reuters *et al.*, *J. Phys. D Appl. Phys.* **47**, 175103 (2014).
12. M. Shatalov *et al.*, *IEEE Electron Device Lett.* **23**, 452–454 (2002).
13. G. Li *et al.*, *IEEE Electron Device Lett.* **34**, 852–854 (2013).
14. A. Nakajima *et al.*, *J. Appl. Phys.* **115**, 153707 (2014).
15. A. Nakajima, Y. Sumida, M. H. Dhyani, H. Kawai, E. M. S. S. Narayanan, *Appl. Phys. Express* **3**, 121004 (2010).
16. Y. Enatsu *et al.*, *Appl. Phys. Express* **9**, 075502 (2016).
17. S. J. Bader *et al.*, *IEEE Electron Device Lett.* **39**, 1848–1851 (2018).
18. S. Birner *et al.*, *IEEE Trans. Electron Dev.* **54**, 2137–2142 (2007).
19. Materials and methods are available as supplementary materials.
20. K. Momma, F. Izumi, *J. Appl. Cryst.* **44**, 1272–1276 (2011).
21. S. J. Bader *et al.*, *Appl. Phys. Lett.* **114**, 253501 (2019).
22. I. P. Smorchkova *et al.*, *J. Appl. Phys.* **86**, 4520–4526 (1999).
23. M. J. Manfra, L. N. Pfeiffer, K. W. West, R. De Picciotto, K. W. Baldwin, *Appl. Phys. Lett.* **86**, 162106 (2005).
24. H. L. Störmer, W. T. Tsang, *Appl. Phys. Lett.* **36**, 685–687 (1980).
25. H. Lee *et al.*, *Nat. Mater.* **17**, 231–236 (2018).
26. T. Yamaguchi *et al.*, *J. Phys. Soc. Jpn.* **82**, 074718 (2013).
27. H. J. Looi, R. B. Jackman, J. S. Foord, *Appl. Phys. Lett.* **72**, 353–355 (1998).
28. K. Hayashi *et al.*, *J. Appl. Phys.* **81**, 744–753 (1997).
29. N. Jiang, T. Ito, *J. Appl. Phys.* **85**, 8267–8273 (1999).
30. M. Kasu, N. Kobayashi, *Appl. Phys. Lett.* **80**, 3961–3963 (2002).
31. M. Myronov, K. Sawano, Y. Shiraki, T. Mouri, K. M. Itoh, *Appl. Phys. Lett.* **91**, 082108 (2007).
32. M. Myronov *et al.*, *Appl. Phys. Lett.* **80**, 3117–3119 (2002).
33. R. J. H. Morris *et al.*, *Semicond. Sci. Technol.* **19**, L106–L109 (2004).
34. H. von Känel *et al.*, *Microelectron. Eng.* **76**, 279–284 (2004).
35. U. König, F. Schaffler, *IEEE Electron Device Lett.* **14**, 205–207 (1993).
36. M. Kaneko, I. Narita, S. Matsumoto, *IEEE Electron Device Lett.* **6**, 575–577 (1985).
37. S. H. Shin, Y. H. Park, H. C. Koo, Y. H. Song, J. D. Song, *Curr. Appl. Phys.* **17**, 1005–1008 (2017).
38. K. Shibata *et al.*, *Appl. Phys. Lett.* **114**, 232102 (2019).
39. M. Karalic *et al.*, *Phys. Rev. B* **99**, 115435 (2019).
40. B. Santic, *Semicond. Sci. Technol.* **18**, 219–224 (2003).
41. S. Nakamura, *Rev. Mod. Phys.* **87**, 1139–1151 (2015).
42. R. Chaudhuri *et al.*, Data for the publication “A polarization-induced 2D hole gas in undoped gallium nitride quantum wells”. Zenodo (2019). doi: 10.5281/zenodo.3245363.

#### ACKNOWLEDGMENTS

The authors thank V. Protasenko, H. Turski, S. M. Islam, K. Lee, and R. Page for help with the MBE operation and A. Mei and K. Shinohara for assistance with measurements. **Funding:** This

work was supported partly by Intel, the Air Force Office of Scientific Research (AFOSR) (grant AFOSR FA9550-17-1-0048), NSF (grants 1710298 and 1534303), and the Cornell Center for Materials Research, with funding from the NSF Materials Research Science and Engineering Center (MRSEC) program (DMR-1719875). Characterizations and measurements were performed in part at the Cornell NanoScale Facility, a National Nanotechnology Coordinated Infrastructure member supported by NSF (grant ECCS-1542081). The presented data made use of the Cornell Center for Materials Research Shared Facilities, which are supported through the NSF MRSEC program (DMR-1719875) and NSF Major Research Instrumentation (DMR-1429155 and DMR-1338010) programs. Z.C. is funded through PARADIM as part of the NSF Materials Innovation Platform program (DMR-1539918). **Author contributions:** R.C. grew and characterized the samples for the study. S.J.B. supported measurements and performed the numerical simulations. Z.C. performed STEM analysis of the heterostructures, under supervision of D.A.M.; R.C., S.J.B., D.J., and H.X. performed experimental data analysis. R.C. and D.J. wrote the manuscript, with inputs from all authors. **Competing interests:** The authors and Cornell University have filed PCT patent application (PCT/US19/42584) on polarization-induced 2DHG for high voltage p-channel transistors. **Data and materials availability:** All data shown in this work are available at Zenodo (42).

#### SUPPLEMENTARY MATERIALS

science.sciencemag.org/content/365/6460/1454/suppl/DC1  
Materials and Methods  
Figs. S1 to S3  
Table S1  
References (43, 44)

22 July 2018; accepted 3 September 2019  
10.1126/science.aau8623

## A polarization-induced 2D hole gas in undoped gallium nitride quantum wells

Reet Chaudhuri, Samuel James Bader, Zhen Chen, David A. Muller, Huili Grace Xing and Debdeep Jena

*Science* **365** (6460), 1454-1457.  
DOI: 10.1126/science.aau8623

### A hole flatland

When two distinct materials are placed on top of each other, the difference in polarization between the two layers can induce charge carriers at the interface. Many such two-dimensional (2D) electron gases have been observed, but engineering a 2D hole gas without the help of doping has been much trickier. Chaudhuri *et al.* used molecular beam epitaxy to grow a layer of gallium nitride on top of aluminum nitride without introducing dopants. This approach resulted in a high-density 2D hole gas at the interface in this technologically relevant system.

*Science*, this issue p. 1454

#### ARTICLE TOOLS

<http://science.sciencemag.org/content/365/6460/1454>

#### SUPPLEMENTARY MATERIALS

<http://science.sciencemag.org/content/suppl/2019/09/25/365.6460.1454.DC1>

#### REFERENCES

This article cites 43 articles, 0 of which you can access for free  
<http://science.sciencemag.org/content/365/6460/1454#BIBL>

#### PERMISSIONS

<http://www.sciencemag.org/help/reprints-and-permissions>

Use of this article is subject to the [Terms of Service](#)

---

*Science* (print ISSN 0036-8075; online ISSN 1095-9203) is published by the American Association for the Advancement of Science, 1200 New York Avenue NW, Washington, DC 20005. The title *Science* is a registered trademark of AAAS.

Copyright © 2019 The Authors, some rights reserved; exclusive licensee American Association for the Advancement of Science. No claim to original U.S. Government Works



Supplementary Material for  
**A polarization-induced 2D hole gas in undoped gallium nitride quantum wells**

Reet Chaudhuri\*, Samuel James Bader, Zhen Chen, David A. Muller, Huili Grace Xing,  
Debdeep Jena

\*Corresponding author. Email: rtc77@cornell.edu

Published 27 September 2019, *Science* **365**, 1454 (2019)  
DOI: 10.1126/science.aau8623

**This PDF file includes:**

Materials and Methods  
Figs. S1 to S3  
Table S1  
References

## Materials and Methods

### Sample Growth

The III-nitride heterostructures studied in this work were epitaxially grown in a Veeco Gen10 plasma-assisted molecular beam epitaxy (PA-MBE) system. Both the doped and undoped GaN/AlN structures were grown on a starting substrate of commercially available 1-micron thick semi-insulating Al-face [0001] AlN on c-plane sapphire templates obtained from DOWA Electronics Materials Co. Ltd. 8 mm × 8 mm diced substrate pieces were ultrasonicated for 10 min each in acetone, methanol and isopropanol in succession before being mounted on a 3-inch lapped Si carrier wafer using molten Indium. The samples were then loaded into the MBE system, and outgassed at 200°C for 8 hours in a load-lock chamber, followed by at 500°C for 2 hours in a clean preparation chamber. They were then introduced into the MBE growth chamber and heated to the desired growth temperature. Effusion cells filled with ultra-high-purity sources were used for Ga, Al and Mg beams, whereas a RF plasma source with ultra-high-purity N<sub>2</sub> gas flowing through a mass-flow-controller and a purifier was used to provide the active N flux. The entire heterostructures reported in this work were grown in a metal-rich condition at a N<sub>2</sub> RF power of 400W, resulting in a growth rate of ~560 nm/hr. A ~400 nm thick AlN buffer was first grown at a thermocouple temperature  $T_{TC} = 780^{\circ}\text{C}$ , with an effective beam-equivalent Al flux of  $\sim 9 \times 10^{-7}$  Torr. Care was taken while growing the AlN buffer to reduce impurity contamination from the substrate surface. In order to maintain an abrupt heterointerface which is important for maximizing the hole mobility, the excess Al on the growth surface was consumed by opening only the N shutter and monitoring the increasing reflection high energy electron diffraction (RHEED) intensity until it saturated. The sample was then cooled to  $T_{TC} = 730^{\circ}\text{C}$  for the growth of the GaN layer. Approximately ~13 nm of unintentionally-doped GaN was grown under an effective Ga flux of

$\sim 1.0 \times 10^{-6}$  Torr. For the undoped structures, the Mg source was kept cold, and the shutter closed throughout, to avoid unintentional Mg doping of the GaN cap layers. On the other hand, for the doped GaN/AlN structures, during the last  $\sim 10$  nm of GaN growth, the hot Mg source shutter was opened to incorporate Mg acceptor dopants. The Mg acceptor concentrations  $N_A$  in the doped samples were verified to be between  $\sim 5 \times 10^{18} \text{ cm}^{-3}$  to  $\sim 1 \times 10^{19} \text{ cm}^{-3}$  in different samples, as calibrated by secondary ion mass spectrometry (SIMS) measurements performed on a separate Mg doping calibration sample grown under the same epitaxial conditions.

### Simulations

All energy band diagrams shown in this work were simulated using a self-consistent multiband  $k \cdot p$  Schrodinger-Poisson solver `nextnano` (18). An undoped GaN layer of varying thickness is assumed strained to a relaxed 500 nm thick, unintentionally-doped AlN (a background n-type doping of  $5 \times 10^{16} \text{ cm}^{-3}$  was assumed). The whole structure is considered metal-polar. The valence band edge is assumed to be 2.9 eV below the Fermi level at the GaN-air surface (surface barrier height for holes) for Fig 1, and is varied for Fig S2. The relevant file for running the simulations are provided at Zenodo (42).

The X-ray diffraction spectrum for fitting to the experimental data were simulated using the open-source Python package `xrayutilities`, the details of which are made available online at Zenodo (42).

### Sample characterizations

Atomic force microscopy (AFM) scans performed in a Bruker ICON Dimension system or an Asylum Cypher system after MBE growth showed a smooth surface with sub-nm rms roughness over both a large area  $10 \mu\text{m} \times 10 \mu\text{m}$  scan and smaller area  $2 \mu\text{m} \times 2 \mu\text{m}$  scans. X-ray diffraction

measurements were performed in a Panalytical XRD system using the Cu-K $\alpha$  line source. A 2 $\theta$ - $\omega$  scan along the (002) symmetric peak of the AlN/GaN structure showed the AlN and GaN reflection peaks and confirmed the thicknesses of the layers by comparing and fitting to a simulated model diffraction spectrum. The reciprocal space map (RSM) around the (105) asymmetric reflection was measured as well. Scanning transmission electron microscopy (STEM) was performed on a probe aberration corrected FEI Titan Themis operating at 300 keV. Thin cross-sectional samples along [110] and [ $\bar{1}$ 10] crystal orientations were prepared using focused ion beam (FIB) and imaged using the annular dark field (ADF) mode of the STEM.

Initial Hall-effect measurements at 300 K and 77 K were performed on all the MBE grown samples using a Nanometric Hall-Effect System, under a 0.32 T magnetic field. Corner ohmic contacts were used to make contact to the samples by using Indium dots in a van der Pauw geometry. One of the doped heterostructure, and one undoped heterostructure were further characterized by measuring the temperature dependent Hall effect from 300 K to 10 K, at 1 T magnetic field in a Lakeshore closed-cycle cryogenic stage. Variation of the Hall resistance  $R_{XY}$  with field was measured by varying the applied normal magnetic field from -1 T to 1 T at 300 K.

### **Supplementary Text**

In a typical metal-rich MBE growth condition, chemical impurities from the substrate surface (Si, O) tend to float on top of the AlN growth front instead of incorporating in the crystal due to unfavorable thermodynamic conditions. They eventually incorporate into the first few layers of Ga-containing AlGaN layers. In the case of the 2DHG structures discussed here, these impurities would incorporate at the buried AlN/GaN interface, where the 2DHG is present – giving rise to compensation, and impurity scattering. It was found that optimized growth modifications in the

form of blocking layers were necessary in the AlN buffer to keep the impurities in the buffer layer. Since this issue is specific to the thermodynamic preferences of impurity incorporation during the metal-rich MBE growth conditions, they may not be essential for obtaining the 2DHG using other epitaxial growth techniques such as metal-organic chemical vapor deposition (MOCVD). It is speculated by the authors that sufficiently suppressing carbon incorporation in MOCVD growth of (AlGa)N might be the key challenge.

AFM scans in Figure 2A clearly show the presence of dislocations in the crystal. The community has long thought that dislocations and other compensating centers whose formation are thermodynamically favored, such as Ga vacancies, preclude the formation of 2D hole gases in GaN heterostructures. But the experimental evidence in this work shows that the polarization discontinuity induces a 2D hole gas despite the presence of dislocations.

The reciprocal space map of X-Ray diffraction spectra of the GaN/AlN epitaxial heterostructure allowed the extraction of the following in-plane and out-of-plane lattice constants:  $a_{AlN} = 0.311$  nm,  $a_{GaN} = 0.311$  nm and  $c_{AlN} = 0.4985$  nm,  $c_{GaN} = 0.5241$  nm. Comparing to the unstrained lattice constants, the GaN layer is under  $\sim 2.41\%$  compressive strain. The wide area STEM scans shown in **Figure S1** confirm the abrupt interface between the GaN and AlN.

The Hall-effect transport data of a selection of MBE grown samples are tabulated in **Table S1**. These samples were grown over different growth days, and illustrate the high repeatability of the properties of the 2D hole gas. These data are used to create the benchmark plot in Figure 4 of the main text. Temperature-dependent Hall-effect measurement studies were done on Samples A4 and B4 in Table S1. These data are presented in Figure 3 of the main text. Although the Mg-doped cap layer in the doped 2DHG structure (sample B in Figure 3) contributes a negligible fraction of mobile holes to the 2D hole gas, it can enable low-resistance tunneling p-type contacts to the 2D

hole gas because of the high electric field it generates near the surface, and thus is investigated here. The control Sample C shows a freeze-out of thermally ionized holes from  $\sim 1.5 \times 10^{13} \text{ cm}^{-2}$  (bulk density of  $\sim 4.1 \times 10^{17} \text{ cm}^{-3}$ ) at 300 K to  $\sim 2 \times 10^{11} \text{ cm}^{-2}$  (bulk density of  $\sim 5.5 \times 10^{15} \text{ cm}^{-3}$ ) at  $\sim 180$  K, making the sample too resistive to measure below  $\sim 180$  K.

**Figure S2** shows the measured variation of the 2D hole gas density with changing GaN layer thickness for an undoped GaN/AlN 2D hole gas heterostructure. **Figure S2A** shows the expected change in the 2D hole gas density with thickness in the energy band diagram of the valence band, and the mobile hole concentration with depth, as simulated using a self-consistent multiband *k.p* Schrodinger-Poisson solver (18). A typical bare-GaN surface valence band edge barrier height of 2.9 eV was used for the simulations in Figure S2A. The solid lines in **Figure S2B** show the expected variation of the polarization-induced hole density versus GaN thickness for various surface barrier heights. For example, for a surface barrier height of  $\sim 3$  eV, the solid lines indicate a critical thickness of  $\sim 4$  nm below which the 2DHG is depleted from the surface potential, a sharp rise in the 2DHG density from  $\sim 5 - 20$  nm, beyond which the hole density saturates to the interface polarization sheet density. The critical thickness is lower for a smaller surface barrier height, reaching  $\sim 1$  nm for a barrier height of 0.6 eV. The measured 2D hole gas densities should follow this trend. To test this, undoped and doped GaN on AlN samples of various thicknesses were grown and their sheet hole densities were measured by Hall-effect at 300 K in a Lakeshore Hall measurement system at a magnetic field of 1 T. The measured 2DHG densities are plotted in **Figure S2B** alongside the solid lines predicted from the polarization discontinuity for various surface barrier heights. We observe a critical GaN thickness of  $\sim 3$  nm, below which no hole gas is measured. The measured 2DHG densities variation with the GaN layer thickness indicates that the surface barrier height may not be fixed, but is likely dependent on the thickness

of the GaN layer, as has previously been observed in 2D electron gases (43, 44). Though the qualitative agreement to the simulated model is a further proof that the 2D hole gas is indeed polarization-induced, it is difficult with the available data to conclusively claim values of the surface barrier height for the doped or undoped samples due to its dependence on variations in epitaxial growth conditions, chemical surface modification due to exposure to atmosphere, etc. Further work is necessary to elucidate the surface Fermi level and its pinning - by either passivating the sample surface in-situ after epitaxy, or by directly measuring the electrical properties of a processed metal-semiconductor Schottky barrier, in both cases ensuring the GaN surface is buried and protected.

Contactless sheet resistance measurement using a Leighton setup was performed (**Figure S3**) on the GaN/AlN structure. Since the instrument can handle only full wafers, a heterostructure with ~15 nm undoped GaN on AlN was grown on a 2-inch substrate wafer (wafer A). A bare substrate wafer without any grown layers was used as a control sample for the measurement (Wafer B). Wafer A showed a sheet resistance in the range of ~16-33 kOhm/sq across the wafer surface. The higher sheet resistance compared to the samples in Fig 3, and the non-uniformity across the surface can be attributed to the growth not being optimized yet for large area substrates. Since the bare substrate wafer was highly resistive (sheet resistance >350 kOhm/sq), we conclude that the conductive 2DHG channel is present in the undoped GaN/AlN heterostructure wafer A. Subsequent Hall-effect measurement results on a diced 8mm × 8mm piece from the wafer with corner Indium contacts corroborate the measured sheet resistance by the contactless method. The presence of the 2D hole gas detected by a contactless measurement is further confirmation of the fact that the holes are polarization-induced, and are not supplied by the metal contacts in a Hall-effect measurement.

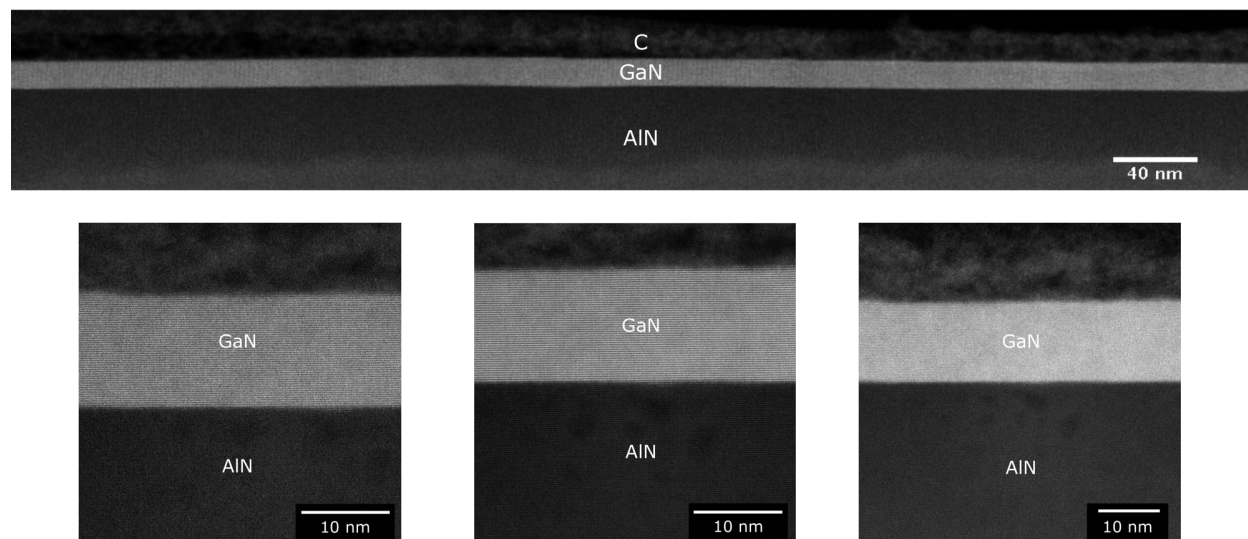


**Fig. S1.**

STEM annular dark field (ADF) images of the cross-section of the GaN/AlN heterostructure along  $[\bar{1}10]$  zone-axis. The wide-area image and the zoomed-in regions clearly show the coherently sharp interface between the GaN and AlN ( $\sim 1$ -2 ML) is maintained over large areas of the wafer, which is essential for a high mobility and high uniformity of the polarization-induced 2D hole gas over the entire wafer.

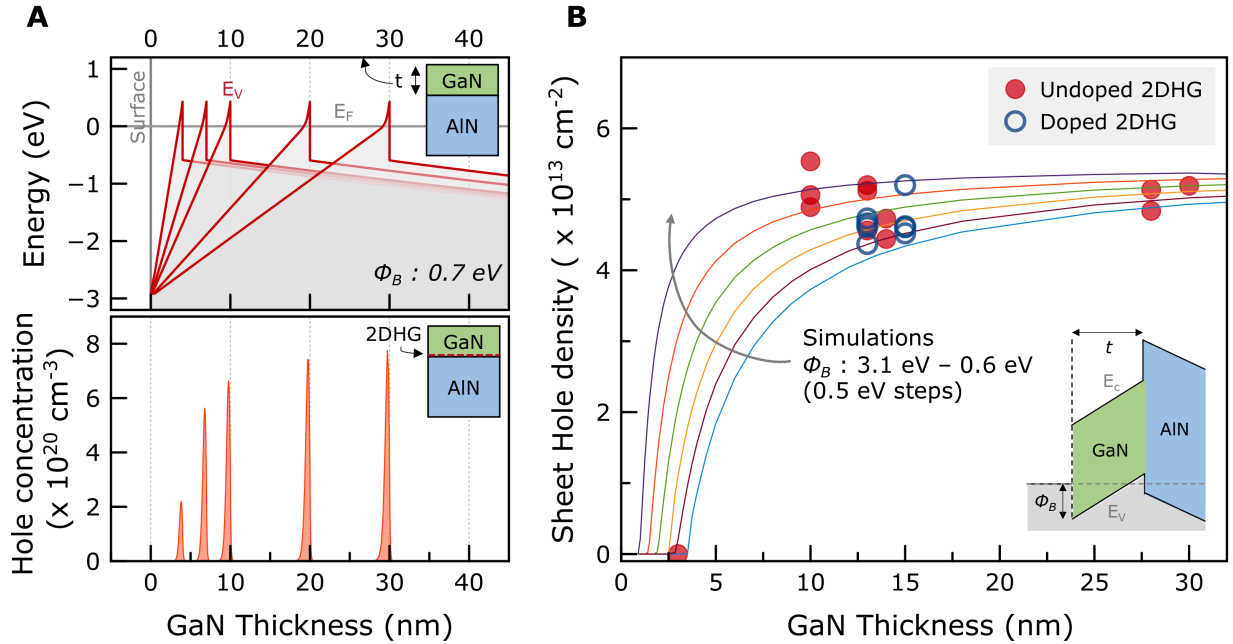


**Fig. S2.**

Dependence of the properties of the polarization-induced 2D hole gas on the thickness of the undoped strained GaN layer grown on AlN. (A) shows the valence band edge and the spatial hole density distribution as a function of the GaN layer thickness. The triangular quantum well at the heterojunction is clearly visible, with the large valence band offset to confine the 2D holes to a width of  $\sim 1$  nm in the vertical direction. The 2D hole gas density increases and saturates for GaN layer thicknesses above  $\sim 30$  nm. (B) shows the measured 2D hole gas densities in various undoped (solid circles) and Mg-doped (hollow circles) GaN/AlN samples with varying GaN thicknesses. The numerical simulations for the variation of the hole gas density with the thickness of the GaN cap layer, for various surface barrier heights is also shown for reference. There clearly exists a critical minimum thickness of GaN for the existence of mobile holes at the GaN/AlN interface - a characteristic of the polarization-induced nature of the 2D hole gas.

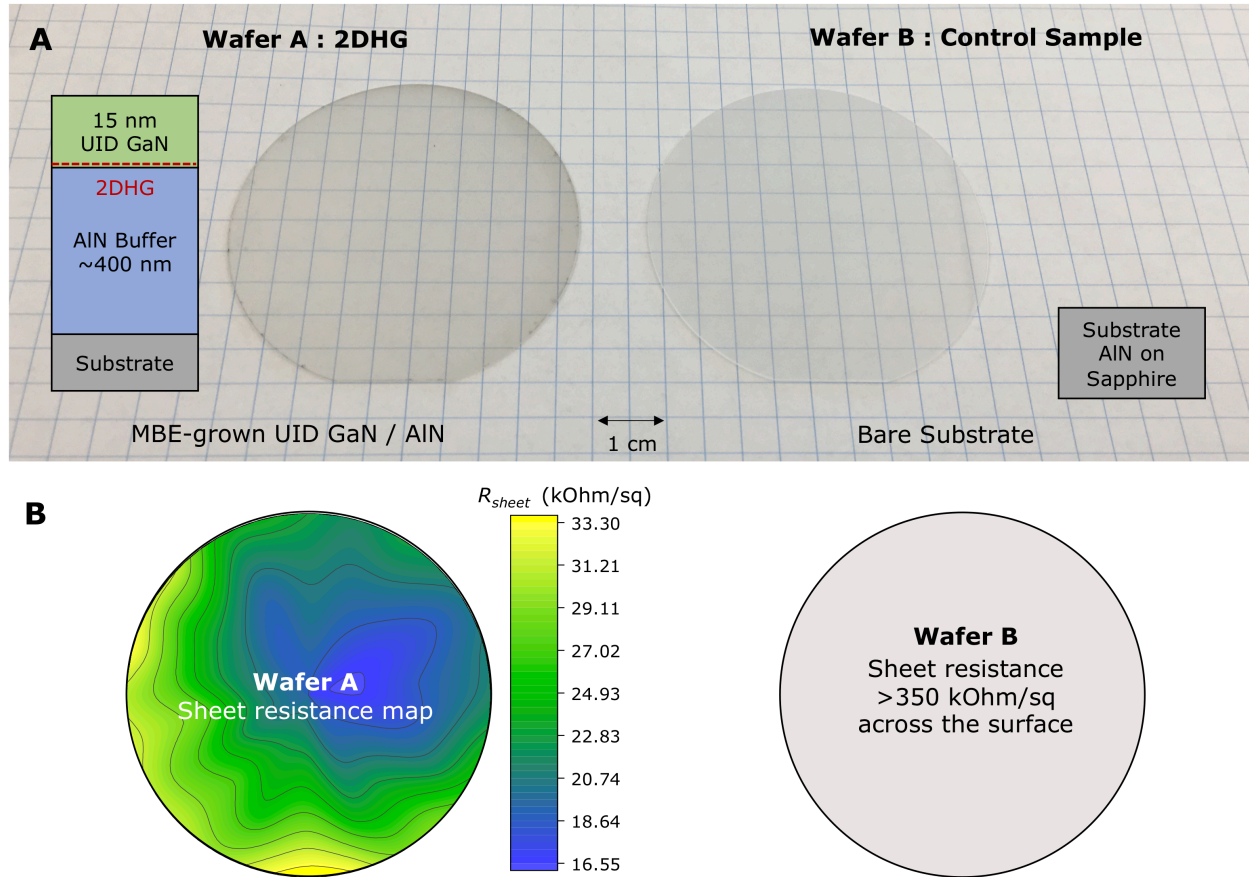


**Fig. S3.**

Contactless sheet resistance measurements of the 2DHG. **(A)** 2-inch MBE-grown GaN/AlN heterostructure wafer with the corresponding layer structure shown, along with a bare substrate wafer used as a control sample **(B)** Sheet resistance map for wafer A shows sheet resistances in the range of ~16-33 kOhm/sq across the surface, whereas wafer B is highly resistive (>350 kOhm/sq). These results confirm the presence of a polarization-induced 2D hole gas as a conductive channel in the undoped heterostructure on wafer A.

<b>Sample</b>	<b>[Mg] in GaN (cm<sup>-3</sup>)</b>	<b>Temp. (K)</b>	<b><math>\mu_{Hall}</math> (cm<sup>2</sup>/V.s)</b>	<b><math>\sigma</math> (cm<sup>-2</sup>)</b>	<b><math>R_{Sheet}</math> (<math>\Omega/\square</math>)</b>
<b>A1</b>	<b>undoped</b>	300	9.28	$5.35 \times 10^{13}$	$1.26 \times 10^4$
		77	40.3	$3.14 \times 10^{13}$	4927
<b>A2</b>	<b>undoped</b>	300	10.1	$5.24 \times 10^{13}$	$1.18 \times 10^4$
		77	48	$2.74 \times 10^{13}$	4751
<b>A3</b>	<b>undoped</b>	300	10.8	$4.66 \times 10^{13}$	$1.24 \times 10^4$
		77	26.3	$5.03 \times 10^{13}$	4715
<b>A4*</b>	<b>undoped</b>	300	23.11	$4.568 \times 10^{13}$	5915
		77	105.8	$3.406 \times 10^{13}$	1733
<b>B1</b>	$1 \times 10^{19}$	300	19.8	$4.66 \times 10^{13}$	6766
		77	78.8	$3.81 \times 10^{13}$	2081
<b>B2</b>	$1 \times 10^{19}$	300	18.6	+4.518e13	7444
		77	79.2	+3.640e13	2166
<b>B3</b>	$1 \times 10^{19}$	300	20.7	$4.73 \times 10^{13}$	6364
		77	71.2	$3.93 \times 10^{13}$	2232
<b>B4*</b>	$5 \times 10^{18}$	300	18.8	$4.37 \times 10^{13}$	7595
		77	102	$3.72 \times 10^{13}$	1647

**Table S1.**

Hall-effect measurement data for several MBE grown 13 nm GaN on AlN heterostructures showing the reproducibility of the 2D hole gas properties in undoped and doped structures. Samples A1-A4 are undoped heterostructures, whereas samples B1-B4 have ~10 nm thick Mg-doped GaN caps on the top of a ~3 nm undoped GaN layer grown on AlN. Samples A4 and B4 were also measured using temperature dependent Hall effect, and are presented in the main text in Figure 3. The data clearly shows the presence of a highly repeatable 2D hole gas, both in the doped and undoped heterostructures.

## References and Notes

1. M. A. Khan, J. N. Kuznia, J. M. Van Hove, N. Pan, J. Carter, Observation of a two-dimensional electron gas in low pressure metalorganic chemical vapor deposited GaN-Al<sub>x</sub>Ga<sub>1-x</sub>N heterojunctions. *Appl. Phys. Lett.* **60**, 3027–3029 (1992). [doi:10.1063/1.106798](https://doi.org/10.1063/1.106798)
2. O. Ambacher, J. Smart, J. R. Shealy, N. G. Weimann, K. Chu, M. Murphy, W. J. Schaff, L. F. Eastman, R. Dimitrov, L. Wittmer, M. Stutzmann, W. Rieger, J. Hilsenbeck, Two-dimensional electron gases induced by spontaneous and piezoelectric polarization charges in N- and Ga-face AlGaIn/GaN heterostructures. *J. Appl. Phys.* **85**, 3222–3233 (1999). [doi:10.1063/1.369664](https://doi.org/10.1063/1.369664)
3. F. Bernardini, V. Fiorentini, D. Vanderbilt, Spontaneous polarization and piezoelectric constants of III-V nitrides. *Phys. Rev. B Condens. Matter* **56**, R10024–R10027 (1997). [doi:10.1103/PhysRevB.56.R10024](https://doi.org/10.1103/PhysRevB.56.R10024)
4. C. Wood, D. Jena, Eds., *Polarization Effects in Semiconductors: From Ab Initio Theory to Device Applications* (Springer, 2007).
5. S. J. Pearton, B. S. Kang, S. Kim, F. Ren, B. P. Gila, C. R. Abernathy, J. Lin, S. N. G. Chu, GaN-based diodes and transistors for chemical, gas, biological and pressure sensing. *J. Phys. Condens. Matter* **16**, R961–R994 (2004). [doi:10.1088/0953-8984/16/29/R02](https://doi.org/10.1088/0953-8984/16/29/R02)
6. U. K. Mishra, L. Shen, T. E. Kazior, Y.-F. Wu, GaN-based RF power devices and amplifiers. *Proc. IEEE* **96**, 287–305 (2008). [doi:10.1109/JPROC.2007.911060](https://doi.org/10.1109/JPROC.2007.911060)
7. T. Zimmermann, M. Neuburger, M. Kunze, I. Daumiller, A. Denisenko, A. Dadgar, A. Krost, E. Kohn, P-channel InGaIn-HFET structure based on polarization doping. *IEEE Electron Device Lett.* **25**, 450–452 (2004). [doi:10.1109/LED.2004.830285](https://doi.org/10.1109/LED.2004.830285)
8. R. Chu, Y. Cao, M. Chen, R. Li, D. Zehnder, An experimental demonstration of GaN CMOS technology. *IEEE Electron Device Lett.* **37**, 269–271 (2016). [doi:10.1109/LED.2016.2515103](https://doi.org/10.1109/LED.2016.2515103)
9. K. Zhang, M. Sumiya, M. Liao, Y. Koide, L. Sang, P-Channel InGaIn/GaN heterostructure metal-oxide-semiconductor field effect transistor based on polarization-induced two-dimensional hole gas. *Sci. Rep.* **6**, 23683 (2016). [doi:10.1038/srep23683](https://doi.org/10.1038/srep23683) [Medline](#)
10. H. Hahn, B. Reuters, A. Pooth, B. Hollander, M. Heuken, H. Kalisch, A. Vescan, P-channel enhancement and depletion mode GaN-based HFETs with quaternary backbarriers. *IEEE Trans. Electron Dev.* **60**, 3005–3011 (2013). [doi:10.1109/TED.2013.2272330](https://doi.org/10.1109/TED.2013.2272330)
11. B. Reuters, H. Hahn, A. Pooth, B. Holländer, U. Breuer, M. Heuken, H. Kalisch, A. Vescan, Fabrication of p-channel heterostructure field effect transistors with polarization-induced two-dimensional hole gases at metal-polar GaN/AlInGaIn interfaces. *J. Phys. D Appl. Phys.* **47**, 175103 (2014). [doi:10.1088/0022-3727/47/17/175103](https://doi.org/10.1088/0022-3727/47/17/175103)
12. M. Shatalov, G. Simin, J. Zhang, V. Adivarahan, A. Koudymov, R. Pachipulusu, M. A. Khan, GaN / AlGaIn p-Channel inverted heterostructure JFET. *IEEE Electron Device Lett.* **23**, 452–454 (2002). [doi:10.1109/LED.2002.801295](https://doi.org/10.1109/LED.2002.801295)

13. G. Li, R. Wang, B. Song, J. Verma, Y. Cao, S. Ganguly, A. Verma, J. Guo, H. G. Xing, D. Jena, Polarization-induced GaN-on-insulator E/D Mode p-channel heterostructure FETs. *IEEE Electron Device Lett.* **34**, 852–854 (2013). [doi:10.1109/LED.2013.2264311](https://doi.org/10.1109/LED.2013.2264311)
14. A. Nakajima, P. Liu, M. Ogura, T. Makino, K. Kakushima, S. I. Nishizawa, H. Ohashi, S. Yamasaki, H. Iwai, Generation and transportation mechanisms for two-dimensional hole gases in GaN/AlGaN/GaN double heterostructures. *J. Appl. Phys.* **115**, 153707 (2014). [doi:10.1063/1.4872242](https://doi.org/10.1063/1.4872242)
15. A. Nakajima, Y. Sumida, M. H. Dhyani, H. Kawai, E. M. S. S. Narayanan, High density two-dimensional hole gas induced by negative polarization at GaN/AlGaN heterointerface. *Appl. Phys. Express* **3**, 121004 (2010). [doi:10.1143/APEX.3.121004](https://doi.org/10.1143/APEX.3.121004)
16. Y. Enatsu, C. Gupta, M. Laurent, S. Keller, S. Nakamura, U. K. Mishra, Polarization induced three-dimensional hole gas in compositionally graded In<sub>x</sub>Ga<sub>1-x</sub>N layer. *Appl. Phys. Express* **9**, 075502 (2016). [doi:10.7567/APEX.9.075502](https://doi.org/10.7567/APEX.9.075502)
17. S. J. Bader, R. Chaudhuri, K. Nomoto, A. Hickman, Z. Chen, H. W. Then, D. A. Muller, H. G. Xing, D. Jena, Gate-recessed E-mode p-channel HFET with high on-current based on GaN/AlN 2D hole gas. *IEEE Electron Device Lett.* **39**, 1848–1851 (2018). [doi:10.1109/LED.2018.2874190](https://doi.org/10.1109/LED.2018.2874190)
18. S. Birner, T. Zibold, T. Andlauer, T. Kubis, M. Sabathil, A. Trellakis, P. Vogl, nextnano: General purpose 3-D simulations. *IEEE Trans. Electron Dev.* **54**, 2137–2142 (2007). [doi:10.1109/TED.2007.902871](https://doi.org/10.1109/TED.2007.902871)
19. Materials and methods are available as supplementary materials.
20. K. Momma, F. Izumi, VESTA 3 for three-dimensional visualization of crystal, volumetric and morphology data. *J. Appl. Cryst.* **44**, 1272–1276 (2011). [doi:10.1107/S0021889811038970](https://doi.org/10.1107/S0021889811038970)
21. S. J. Bader, R. Chaudhuri, M. Schubert, H. W. Then, H. G. Xing, D. Jena, Wurtzite phonons and the mobility of a GaN/AlN 2D hole gas. *Appl. Phys. Lett.* **114**, 253501 (2019).
22. I. P. Smorchkova, C. R. Elsass, J. P. Ibbetson, R. Vetury, B. Heying, P. Fini, E. Haus, S. P. DenBaars, J. S. Speck, U. K. Mishra, Polarization-induced charge and electron mobility in AlGaN/GaN heterostructures grown by plasma-assisted molecular-beam epitaxy. *J. Appl. Phys.* **86**, 4520–4526 (1999). [doi:10.1063/1.371396](https://doi.org/10.1063/1.371396)
23. M. J. Manfra, L. N. Pfeiffer, K. W. West, R. De Picciotto, K. W. Baldwin, High mobility two-dimensional hole system in GaAs/AlGaAs quantum wells grown on (100) GaAs substrates. *Appl. Phys. Lett.* **86**, 162106 (2005). [doi:10.1063/1.1900949](https://doi.org/10.1063/1.1900949)
24. H. L. Störmer, W. T. Tsang, Two-dimensional hole gas at a semiconductor heterojunction interface. *Appl. Phys. Lett.* **36**, 685–687 (1980). [doi:10.1063/1.91624](https://doi.org/10.1063/1.91624)
25. H. Lee, N. Campbell, J. Lee, T. J. Asel, T. R. Paudel, H. Zhou, J. W. Lee, B. Noesges, J. Seo, B. Park, L. J. Brillson, S. H. Oh, E. Y. Tsympal, M. S. Rzchowski, C. B. Eom, Direct observation of a two-dimensional hole gas at oxide interfaces. *Nat. Mater.* **17**, 231–236 (2018). [doi:10.1038/s41563-017-0002-4](https://doi.org/10.1038/s41563-017-0002-4) [Medline](#)
26. T. Yamaguchi, E. Watanabe, H. Osato, D. Tsuya, K. Deguchi, T. Watanabe, H. Takeya, Y. Takano, S. Kurihara, H. Kawarada, Low-temperature transport properties of holes

- introduced by ionic liquid gating in hydrogen-terminated diamond surfaces. *J. Phys. Soc. Jpn.* **82**, 074718 (2013). [doi:10.7566/JPSJ.82.074718](https://doi.org/10.7566/JPSJ.82.074718)
27. H. J. Looi, R. B. Jackman, J. S. Foord, High carrier mobility in polycrystalline thin film diamond. *Appl. Phys. Lett.* **72**, 353–355 (1998). [doi:10.1063/1.120734](https://doi.org/10.1063/1.120734)
  28. K. Hayashi, S. Yamanaka, H. Watanabe, T. Sekiguchi, H. Okushi, K. Kajimura, Investigation of the effect of hydrogen on electrical and optical properties in chemical vapor deposited on homoepitaxial diamond films. *J. Appl. Phys.* **81**, 744–753 (1997). [doi:10.1063/1.364299](https://doi.org/10.1063/1.364299)
  29. N. Jiang, T. Ito, Electrical properties of surface conductive layers of homoepitaxial diamond films. *J. Appl. Phys.* **85**, 8267–8273 (1999). [doi:10.1063/1.370668](https://doi.org/10.1063/1.370668)
  30. M. Kasu, N. Kobayashi, High hole mobility ( $1300\text{cm}^2/\text{Vs}$ ) at room temperature in hydrogen-terminated (001) diamond. *Appl. Phys. Lett.* **80**, 3961–3963 (2002). [doi:10.1063/1.1481535](https://doi.org/10.1063/1.1481535)
  31. M. Myronov, K. Sawano, Y. Shiraki, T. Mouri, K. M. Itoh, Observation of two-dimensional hole gas with mobility and carrier density exceeding those of two-dimensional electron gas at room temperature in the SiGe heterostructures. *Appl. Phys. Lett.* **91**, 082108 (2007). [doi:10.1063/1.2773744](https://doi.org/10.1063/1.2773744)
  32. M. Myronov, T. Irisawa, O. A. Mironov, S. Koh, Y. Shiraki, T. E. Whall, E. H. C. Parker, Extremely high room-temperature two-dimensional hole gas mobility in Ge/Si<sub>0.33</sub>Ge<sub>0.67</sub>/Si(001) p-type modulation-doped heterostructures. *Appl. Phys. Lett.* **80**, 3117–3119 (2002). [doi:10.1063/1.1473690](https://doi.org/10.1063/1.1473690)
  33. R. J. H. Morris, T. J. Grasby, R. Hammond, M. Myronov, O. A. Mironov, D. R. Leadley, T. E. Whall, E. H. C. Parker, M. T. Currie, C. W. Leitz, E. A. Fitzgerald, High conductance Ge p-channel heterostructures realized by hybrid epitaxial growth. *Semicond. Sci. Technol.* **19**, L106–L109 (2004). [doi:10.1088/0268-1242/19/10/L03](https://doi.org/10.1088/0268-1242/19/10/L03)
  34. H. von Känel, D. Chrastina, B. Rössner, G. Isella, J. P. Hague, M. Bollani, High mobility SiGe heterostructures fabricated by low-energy plasma-enhanced chemical vapor deposition. *Microelectron. Eng.* **76**, 279–284 (2004). [doi:10.1016/j.mee.2004.07.029](https://doi.org/10.1016/j.mee.2004.07.029)
  35. U. König, F. Schaffler, p-Type Ge-channel MODFET's with high transconductance grown on Si substrates. *IEEE Electron Device Lett.* **14**, 205–207 (1993). [doi:10.1109/55.215149](https://doi.org/10.1109/55.215149)
  36. M. Kaneko, I. Narita, S. Matsumoto, The study on hole mobility in the inversion layer of P-channel MOSFET. *IEEE Electron Device Lett.* **6**, 575–577 (1985). [doi:10.1109/EDL.1985.26235](https://doi.org/10.1109/EDL.1985.26235)
  37. S. H. Shin, Y. H. Park, H. C. Koo, Y. H. Song, J. D. Song, GaSb/InGaAs 2-dimensional hole gas grown on InP substrate for III-V CMOS applications. *Curr. Appl. Phys.* **17**, 1005–1008 (2017). [doi:10.1016/j.cap.2017.03.018](https://doi.org/10.1016/j.cap.2017.03.018)
  38. K. Shibata, M. Karalic, C. Mittag, T. Tschirky, C. Reichl, H. Ito, K. Hashimoto, T. Tomimatsu, Y. Hirayama, W. Wegscheider, T. Ihn, K. Ensslin, Electric-field-induced two-dimensional hole gas in undoped GaSb quantum wells. *Appl. Phys. Lett.* **114**, 232102 (2019). [doi:10.1063/1.5093133](https://doi.org/10.1063/1.5093133)

39. M. Karalic, C. Mittag, M. Hug, T. Tschirky, W. Wegscheider, K. Ensslin, T. Ihn, K. Shibata, R. Winkler, Gate-tunable electronic transport in p-type GaSb quantum wells. *Phys. Rev. B* **99**, 115435 (2019). [doi:10.1103/PhysRevB.99.115435](https://doi.org/10.1103/PhysRevB.99.115435)
40. B. Santic, On the hole effective mass and the free hole statistics in wurtzite GaN. *Semicond. Sci. Technol.* **18**, 219–224 (2003). [doi:10.1088/0268-1242/18/4/305](https://doi.org/10.1088/0268-1242/18/4/305)
41. S. Nakamura, Nobel Lecture: Background story of the invention of efficient blue InGaN light emitting diodes. *Rev. Mod. Phys.* **87**, 1139–1151 (2015). [doi:10.1103/RevModPhys.87.1139](https://doi.org/10.1103/RevModPhys.87.1139) [Medline](#)
42. R. Chaudhuri, S. J. Bader, Z. Chen, D. A. Muller, H. G. Xing, D. Jena, Data for the publication “A polarization-induced 2D hole gas in undoped gallium nitride quantum wells”. Zenodo (2019), DOI: [10.5281/zenodo.3245363](https://doi.org/10.5281/zenodo.3245363).
43. G. Li, Y. Cao, H. G. Xing, D. Jena, High mobility two-dimensional electron gases in nitride heterostructures with high Al composition AlGa<sub>N</sub> alloy barriers. *Appl. Phys. Lett.* **97**, 222110 (2010). [doi:10.1063/1.3523358](https://doi.org/10.1063/1.3523358)
44. K. Köhler, S. Müller, R. Aidam, P. Waltereit, W. Pletschen, L. Kirste, H. P. Menner, W. Bronner, A. Leuther, R. Quay, M. Mikulla, O. Ambacher, R. Granzner, F. Schwierz, C. Buchheim, R. Goldhahn, Influence of the surface potential on electrical properties of Al<sub>x</sub>Ga<sub>1-x</sub>N/GaN heterostructures with different Al-content: Effect of growth method. *J. Appl. Phys.* **107**, 053711 (2010). [doi:10.1063/1.3319585](https://doi.org/10.1063/1.3319585)